

Gd³⁺ as a probing and tuning tool of strong electronic correlations in the heavy-fermion Kondo lattice compound YbFe₂Zn₂₀M. Cabrera-Baez,¹ M. A. Avila,² and C. Rettori^{1,2}¹*Instituto de Física “Gleb Wataghin,” UNICAMP, Campinas, SP, 13083-859 Brazil*²*CCNH, Universidade Federal do ABC (UFABC), Santo André, SP, 09210-580 Brazil*

(Received 22 May 2018; revised manuscript received 19 September 2018; published 3 October 2018)

We report on the magnetic, thermodynamic, and electronic properties of the Gd-doped Kondo-lattice compound YbFe₂Zn₂₀ ($T_K \approx 32$ K) by means of T -dependent magnetization, specific heat, and electron spin resonance (ESR) measurements. As Gd is incorporated in this system (Yb_{1-x}Gd_xFe₂Zn₂₀), the Yb contribution to the Sommerfeld coefficient remains almost unaltered for $x = 0.005$ and 0.01 at $\gamma_{\text{eff}} \approx 500$ mJ mol⁻¹ K⁻², however, for $x = 0.05$, it is reduced to $\gamma_{\text{eff}} = 450$ mJ mol⁻¹ K⁻². As expected for heavy-fermion systems, the Gd³⁺ ESR experiments show an enhanced Korringa relaxation rate, $b = d(\Delta H)/(dT)$, due to the exchange interaction between the Gd³⁺ localized magnetic moment and the high $4f$ -conduction electrons (ce) density of states at the Fermi level. Below T_K , the Gd³⁺ ESR g shift presents a peculiar T dependence. For $x \lesssim 0.01$, we associate the g shift to an internal molecular AFM field due to the ce screening of the Yb³⁺ magnetic moments in the Kondo condensate with a value of $\lambda = -2.80(1)$ mol Oe/emu. The negative value reflects a singlet nonmagnetic ground-state formation, consistent with a Kondo-lattice system. Still below T_K , but for $x = 0.05$, the Gd³⁺ ESR g shift presents a positive T dependence, which we now associate to an internal molecular FM field due to a Gd³⁺-Gd³⁺ superexchange-like interaction via extended Fe $3d$ ce . A Fermi surface reconstruction process is found to take place in the crossover from the high- T to low- T regimes, such that a momentum transfer dependence of the Gd³⁺- ce exchange interaction [$J_{f-ce}(q)$] in the former is lost as the Kondo condensate sets in.

DOI: [10.1103/PhysRevB.98.165106](https://doi.org/10.1103/PhysRevB.98.165106)**I. INTRODUCTION**

Heavy-fermion rare-earth (RE) based compounds are considered fundamental systems to investigate the properties of strongly correlated electrons [1–3]. One of their most important features is the enhanced density of states at the Fermi level, leading to an electron mass renormalization due to the $4f$ hybridization with the conduction electrons (ce) [1–5]. A clear experimental manifestation of the above effect is the large value of the Sommerfeld coefficient γ when compared with a reference compound lacking $4f$ -type electrons close to the Fermi surface.

As is well known, Yb-based compounds can show a full range of magnetic ground states depending on how its $4f$ levels are situated with respect to the Fermi level and the ce . There are metallic systems with a well defined Yb²⁺ valence, resulting in a Pauli-like magnetic susceptibility with γ values comparable to common metals [6]. In some cases, the compounds are characterized by moderate values of γ (50–100 mJ mol⁻¹ K⁻²) such as Yb₂TGe₆ compounds [7] (T = transition metals), showing Yb²⁺-Yb³⁺ valence fluctuating features. In other cases, the compounds are well defined heavy-fermion systems, with the Yb valence very close to 3+, leading to large values of γ and Kondo-like behavior at low T , as in YbNiSi₃ [8], Yb₂Ni₁₂P₇ [9], and YbT₂Zn₂₀ [5]. In particular, YbFe₂Zn₂₀ and YbCo₂Zn₂₀ were classified as heavy-fermion systems [5] with γ values of 530 and 7900 mJ mol⁻¹ K⁻², respectively. The large values for YbFe₂Zn₂₀ and YbCo₂Zn₂₀ compounds are due to the proximity of the Yb $4f$ states to the Fermi level, as revealed by DFT calculations [10].

Assuming an electronic mass renormalization framework, the Fermi liquid description of the specific heat follows the usual T dependence [1–3], $C_p = \gamma^*T + \beta T^3$, modified only by an enhanced γ^* value, which was observed in YbFe₂Zn₂₀ but for YbCo₂Zn₂₀, a strong divergence of C_p/T occurs as T approaches 0 K [5,11]. Another remarkable difference between these two strongly correlated systems is the T dependence of the dc magnetic susceptibility, with a clear loss of local moment at low- T for YbFe₂Zn₂₀ and Curie-Weiss-like behavior for YbCo₂Zn₂₀ [5]. The above differences point toward YbFe₂Zn₂₀ ($T_K \approx 32$ K) being a good Kondo lattice candidate to explore strongly correlated properties involving microscopic techniques where the Fermi liquid formalism is normally applicable.

One useful technique to explore systems from a microscopic point of view is the electron spin resonance (ESR) that uses a magnetic probe to extract information on the magnetic interactions between the local probe (f or d type of localized electrons) and the ce [12–14]. Such microscopic characterizations in this family have been previously conducted on GdCo₂Zn₂₀ and GdFe₂Zn₂₀, probing a range of interactions from AFM in the former [15] to FM in the latter [16], where the $4f$ - ce interplay is fundamental in establishing the magnetic order. For ESR of localized magnetic moments in metallic hosts, the exchange interaction between the impurity magnetic moment and the ce can be estimated from the T dependence of the linewidth, $\frac{d(\Delta H)}{dT}$, and g shift, Δg [$\Delta g = g - 1.993(2)$], provided that the density of states (DOS) at the Fermi level is known [17]. Thus ESR parameters are expected to be strongly affected in a heavy-fermion system.

With the intent of expanding the advances reached in Gd-based compounds into the hybridized members of the family, we have grown single crystals of $\text{Yb}_{1-x}\text{Gd}_x\text{Fe}_2\text{Zn}_{20}$ with $0 \lesssim x \lesssim 0.05$ (and $\text{Y}_{1-x}\text{Gd}_x\text{Fe}_2\text{Zn}_{20}$ as reference compounds) to study the effects of electronic correlations on the T behavior of the Gd^{3+} local magnetic moments by means of ESR, magnetization, and specific heat experiments. The combined experiments show that the Korringa relaxation $b = \frac{d(\Delta H)}{dT}$ in $\text{Yb}_{1-x}\text{Gd}_x\text{Fe}_2\text{Zn}_{20}$ is enhanced five-fold relative to that of $\text{Y}_{1-x}\text{Gd}_x\text{Fe}_2\text{Zn}_{20}$ for $x = 0.05$, evidencing the expected increase of the DOS at the Fermi level due to the proximity of Yb 4*f*-type electrons that gain partial itinerant character. The T dependence of the Gd^{3+} g shift (Δg_{eff}) is unique in showing two opposite trends at low- T (2–18 K), which reflect those in the dc magnetic susceptibility of $\text{Yb}_{1-x}\text{Gd}_x\text{Fe}_2\text{Zn}_{20}$. Our analyses suggest that the Gd^{3+} ions are probing an internal molecular magnetic field of two different origins, a Kondo-like AFM combined with FM-like couplings. Then, assuming that $g_{\text{eff}} = g(1 + \lambda\chi_{\text{Yb;Gd}})$, we estimate the molecular field parameter involving the exchange interaction from both mechanisms.

II. EXPERIMENTS

Several batches of $\text{Yb}_{1-x}\text{Gd}_x\text{Fe}_2\text{Zn}_{20}$ and $\text{Y}_{1-x}\text{Gd}_x\text{Fe}_2\text{Zn}_{20}$ single crystals were grown with $0 \lesssim y \lesssim 0.05$ by the standard self-flux method [18,19] using excess Zn. The constituent elements were 99.99% Yb (Ames) and 99.9% Y, 99.9% Gd, 99.9% Fe, and 99.9999% Zn (Alfa-Aesar). The initial ratios of elements were 1:2:47 for the ternaries Y:Fe:Zn and Yb:Fe:Zn, and $1 - x:x:2:47$ for the pseudoquaternaries Y:Gd:Fe:Zn and Yb:Gd:Fe:Zn. The initial reagents were sealed in an evacuated quartz ampoule and heated in a box furnace. Crystals were grown by slowly cooling the melt between 1100 °C and 600 °C over 100 h. At 600 °C, the ampoules were removed from the furnace, inverted, and placed in a centrifuge to spin off the excess flux. The Gd concentration was estimated using dc magnetic susceptibility measurements combining proportional amounts of Gd and Yb to fit the total value of the effective magnetic moment. The estimated Gd concentrations were in very good agreement with the nominal ones for all samples. X-ray diffraction (XRD) of crushed crystals at room- T was performed to determine the crystal structures, which matched the cubic $\text{CeCr}_2\text{Al}_{20}$ type [20,21,24]. A Quantum Design MPMS3 SQUID-VSM magnetometer was used for magnetic susceptibility ($\chi = M/H$) measurements at various applied magnetic fields ($H \leq 3$ T) and temperatures ($2.0 \text{ K} \leq T \leq 310 \text{ K}$). The T -dependent specific heat (C_p) was measured in a Quantum Design PPMS platform using the relaxation technique at zero field. For the ESR experiments, single crystals were crushed into powders of particle size greater than 100 μm , corresponding to an average grain size (d) larger than the skin depth (δ), $\lambda = d/\delta \gtrsim 10$. The x-band ($\nu \approx 9.4$ GHz) ESR experiments were carried out in a conventional CW Bruker-ELEXSYS 500 ESR spectrometer using a TE₁₀₂ cavity. The sample temperature was changed using a helium gas-flux coupled to an Oxford T controller.

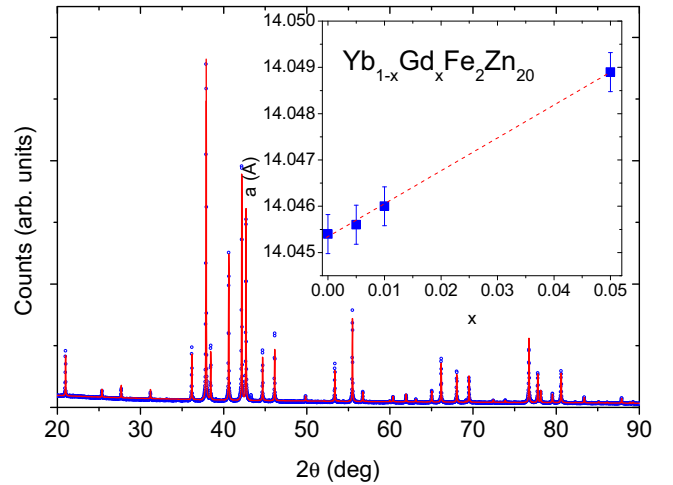


FIG. 1. X-ray diffraction pattern of $\text{YbFe}_2\text{Zn}_{20}$. (Inset) Evolution of the cubic lattice parameter for the $\text{Yb}_{1-x}\text{Gd}_x\text{Fe}_2\text{Zn}_{20}$ ($0 \lesssim x \lesssim 0.05$) compounds.

III. EXPERIMENTAL RESULTS

The XRD pattern of $\text{YbFe}_2\text{Zn}_{20}$ is displayed in Fig. 1. It is consistent with the cubic $\text{CeCr}_2\text{Al}_{20}$ -type structure, and the inset shows that the Gd-concentration dependence of the refined lattice parameter a , extracted from the patterns of all other samples, follows Vegard's law as expected.

The presence of diluted Gd^{3+} local magnetic moments in the heavy-fermion $\text{YbFe}_2\text{Zn}_{20}$ is manifested in the low- T Curie-like dc magnetic susceptibility data shown in Fig. 2(a), for different concentrations ($0 \lesssim x \lesssim 0.05$). High- T Curie-Weiss fitting of the inverse dc magnetic susceptibility for all samples [Fig. 2(b)] allow extraction of the effective magnetic moments corresponding to the actual compositions of Yb and Gd in each case. The fittings also reveal an evolution of the Curie-Weiss parameter θ_{CW} , from -17 K for $x = 0$ to 0 K for $x = 0.05$. The data of Fig. 2 show a subtle interplay between Yb^{3+} - Yb^{3+} AFM coupling and Gd^{3+} - Gd^{3+} FM interaction within a very small range of Gd concentration, $0 \lesssim x \lesssim 0.05$. The evolution of the system's magnetic response from paramagnetic for $x = 0$ to ferromagnetic for $x = 0.05$ is evidenced in Fig. 3, which displays the low- T magnetization isotherms ($M \times H$). Notice that the compound $\text{GdFe}_2\text{Zn}_{20}$ ($x = 1.00$) is a FM with $T_C = 86$ K [21].

The introduction of Gd^{3+} ions affects the system not only magnetically but also thermodynamically. Figure 4(a) shows $C_p/T \times T^2$ for $\text{Yb}_{1-x}\text{Gd}_x\text{Fe}_2\text{Zn}_{20}$ ($0 \lesssim x \lesssim 0.05$) where an increase of the Sommerfeld coefficient (extrapolated from $C_p/T|_{T=0}$) is observed, from $\gamma = 530 \text{ mJ mol}^{-1} \text{ K}^{-2}$ for $x = 0$ to $670 \text{ mJ mol}^{-1} \text{ K}^{-2}$ for $x = 0.05$. For comparison, the same plot for the reference samples $\text{Y}_{1-x}\text{Gd}_x\text{Fe}_2\text{Zn}_{20}$ is presented in Fig. 4(b), where the extrapolated values vary from 50 to $220 \text{ mJ mol}^{-1} \text{ K}^{-2}$, respectively.

To further explore the interplay between the AFM and FM coupling in this heavy-fermion system microscopically, we have performed ESR experiments at different temperatures in the same set of $\text{Yb}_{1-x}\text{Gd}_x\text{Fe}_2\text{Zn}_{20}$ batches. Figure 5(a) shows the measured ESR of Gd^{3+} in $\text{Yb}_{0.995}\text{Gd}_{0.005}\text{Fe}_2\text{Zn}_{20}$ at $T \approx 4$ K and $P_{\mu\text{w}} = 2$ mW. Fitting a Dyson line shape [22,23]

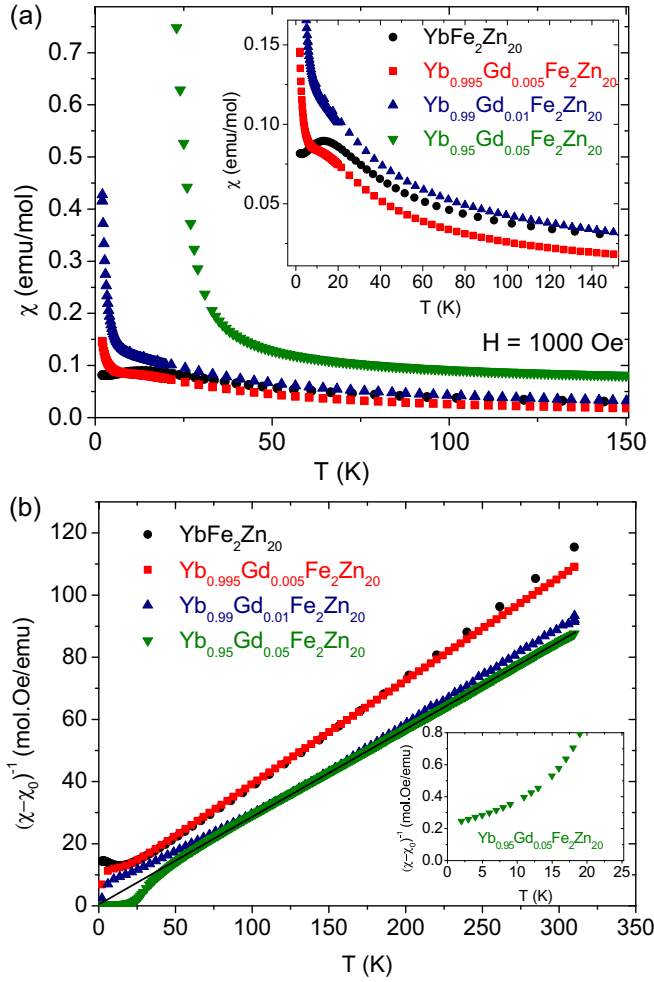


FIG. 2. T dependence of (a) the dc magnetic susceptibility and (b) the inverse susceptibility for $\text{Yb}_{1-x}\text{Gd}_x\text{Fe}_2\text{Zn}_{20}$ ($0 \lesssim x \lesssim 0.05$) at $H = 1000$ Oe. The inset in (b) shows a zoom at low T .

(black line) yields a negative g shift [$\Delta g = g - 1.993(2) = -0.051(3)$] and a linewidth of $\Delta H \approx 211(20)$ Oe. It is worth mentioning that no ESR signal was detected for the undoped sample, $\text{YbFe}_2\text{Zn}_{20}$.

After repeating the measurements and fittings for all samples at several temperatures, a striking T dependence of Δg was found [Fig. 5(b)]. $\text{Yb}_{0.995}\text{Gd}_{0.005}\text{Fe}_2\text{Zn}_{20}$ and $\text{Yb}_{0.99}\text{Gd}_{0.01}\text{Fe}_2\text{Zn}_{20}$ show small negative values within the respective low- T ranges, where ESR signals could be experimentally observed, whereas $\text{Yb}_{0.95}\text{Gd}_{0.05}\text{Fe}_2\text{Zn}_{20}$ presents a crossover from negative values at high T to positive ones below $T \approx 25$ K, signaling different acting mechanisms upon cooling. With respect to the T dependence of the Gd^{3+} ESR linewidth [Fig. 5(c)], ΔH for $\text{Yb}_{0.995}\text{Gd}_{0.005}\text{Fe}_2\text{Zn}_{20}$, $\text{Yb}_{0.99}\text{Gd}_{0.01}\text{Fe}_2\text{Zn}_{20}$, and $\text{Yb}_{0.95}\text{Gd}_{0.05}\text{Fe}_2\text{Zn}_{20}$ show similar linear slopes, which result in similar values for the Korringa relaxation rates, $b = 49(3)$, $54(3)$, and $50(3)$ Oe/K, respectively.

Once again for comparison, the Gd^{3+} ESR experiments were repeated for the nonhybridizing reference compound $\text{Y}_{0.95}\text{Gd}_{0.05}\text{Fe}_2\text{Zn}_{20}$. The T dependencies of the ESR parameters ΔH (Fig. 6) and Δg (inset) lead to a significantly smaller

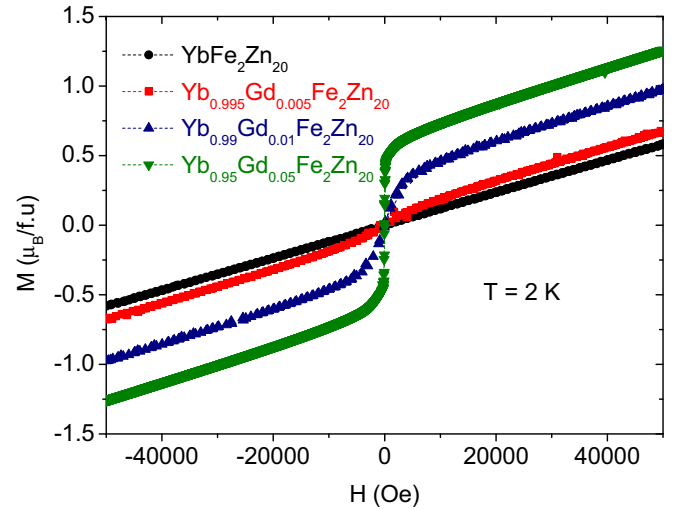


FIG. 3. Magnetic isotherms for $\text{Yb}_{1-x}\text{Gd}_x\text{Fe}_2\text{Zn}_{20}$ ($0 \lesssim x \lesssim 0.05$) at $T = 2$ K.

Korringa relaxation rate of $b = 11(1)$ Oe/K, and to negative g shifts of order $\Delta g = -0.10(2)$ at low T , comparable to those at high T of the Yb-based sample with the same Gd concentration.

IV. ANALYSIS AND DISCUSSION

It is evident from the set of data presented in the previous section that strong electronic correlation effects can be probed by different low Gd^{3+} doping concentrations in $\text{YbFe}_2\text{Zn}_{20}$. Let us start by analyzing the specific heat results within the framework of such correlations. The low- T linear behavior of $C_p/T = \gamma^* + \beta T^2$ for $\text{Yb}_{1-x}\text{Gd}_x\text{Fe}_2\text{Zn}_{20}$ [Fig. 4(a)] leads to an enhancement of the Sommerfeld coefficient as a function of the Gd content. This is an unexpected result since the substitution should be removing Yb $4f$ - ce from the Fermi level and introducing the localized Gd $4f$ electrons. The puzzle may be resolved by the response of the reference compound $\text{Y}_{1-x}\text{Gd}_x\text{Fe}_2\text{Zn}_{20}$ with the same Gd^{3+} concentration, which also reveals an increase in γ . In this case, it is clearly associated to an enhancement of magnetic entropy and consequently of the magnetic component in the specific heat C_{mag} rather than mass renormalization effects. Hence proper analysis of the electronic effects in the heavy-fermion system requires evaluation of a reduced *effective* Sommerfeld coefficient, $\gamma_{\text{Gd:Yb}}^{\text{eff}} = \gamma_{\text{Gd:Yb}} - \gamma_{\text{Gd:Y}}$. This “corrected” electronic parameter will be important later in our discussion of the $\text{Yb}_{0.99}\text{Gd}_{0.01}\text{Fe}_2\text{Zn}_{20}$ sample behavior.

Now let us analyze the magnetic effects. The T -dependent magnetic susceptibility and its inverse (Fig. 2) for $\text{Yb}_{1-x}\text{Gd}_x\text{Fe}_2\text{Zn}_{20}$ reveal a competition between AFM and FM interactions. The Curie-Weiss parameter is negative for $x = 0$ ($\theta_{\text{CW}} = -17$ K), corresponding to AFM coupling between Yb-Yb and leading to an effective negative exchange $J_{\text{Yb-Yb}}^{\text{eff}}$. With increasing Gd concentration, θ_{CW} decreases until it essentially vanishes for $x = 0.05$, leading to $J_{\text{Yb-Yb}}^{\text{eff}} \sim 0$. However, the magnetic isotherms (Fig. 3) make it clear that such suppression is not due to weakening of the AFM interaction, but rather that the system acquires an increasingly

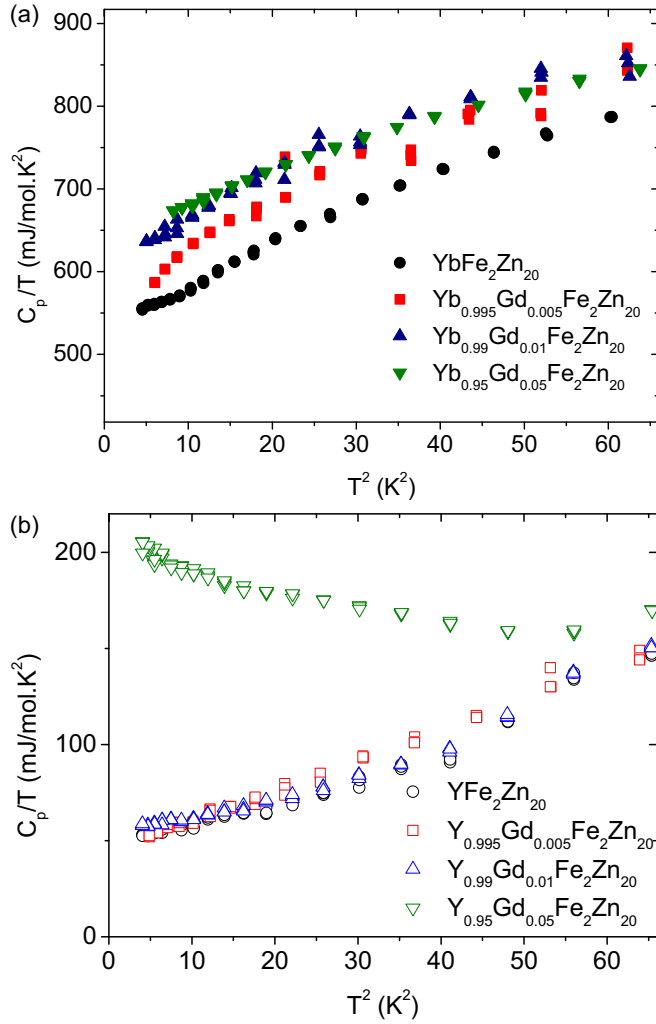


FIG. 4. $C_p/T \times T^2$ for (a) $\text{Yb}_{1-x}\text{Gd}_x\text{Fe}_2\text{Zn}_{20}$ and (b) $\text{Y}_{1-x}\text{Gd}_x\text{Fe}_2\text{Zn}_{20}$ with $0 \lesssim x \leq 0.05$.

relevant FM component. This FM behavior is presumably associated to Gd-Gd interaction, yet different from that reported in the reference system $\text{Y}_{1-x}\text{Gd}_x\text{Fe}_2\text{Zn}_{20}$ [21], where $4f$ - ce are absent.

Therefore the magnetic behavior indicates that long-range FM and short-range Kondo-like interactions should coexist and be competing in the heavy-fermion system. A microscopic characterization of these magnetic interactions may then help understand such competition. ESR of rare-earth ions diluted in metallic hosts is a useful local technique to investigate the properties of materials, since it directly probes the nature of the interactions between the localized magnetic moment and its neighborhood. To avoid CEF effects, $\text{Gd}^{3+} 4f^7 (L=0)$ was chosen as an ideal probe to explore noncorrelated systems [15,25] and also Stoner-type correlated systems of this family [16]. A Dysonian fitting of the T -dependent ESR results in all our samples allowed extraction of the two most important observables, the linewidth, ΔH , and the g shift, Δg [as exemplified in Fig. 5(a)], given by Refs. [17,26],

$$\Delta g = J_{f,ce}(0)\eta_F \quad (1)$$

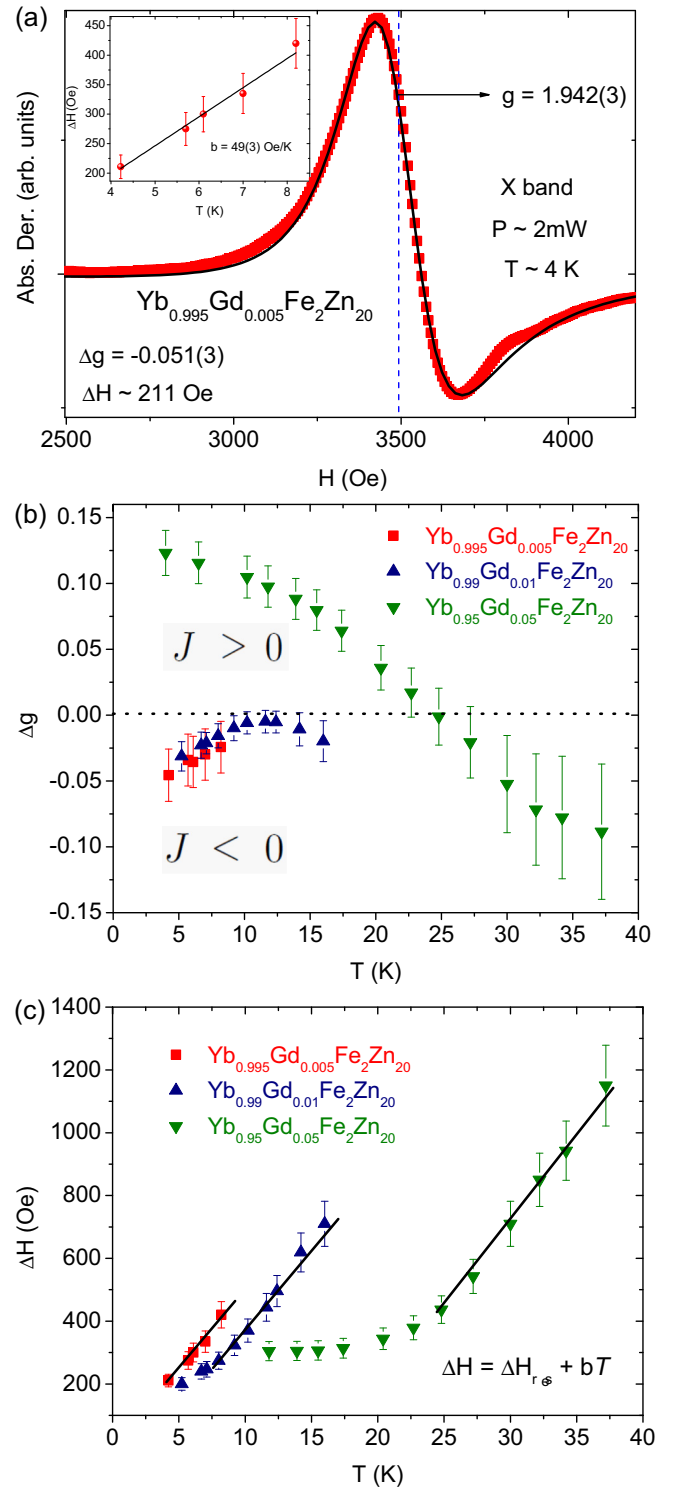


FIG. 5. (a) Resonance signal of Gd^{3+} in $\text{Yb}_{0.995}\text{Gd}_{0.005}\text{Fe}_2\text{Zn}_{20}$ with $g = 1.942(3)$ at $T = 4$ K. The inset presents the T dependence of the extracted linewidth. (b) and (c) present the extracted Δg and ΔH ESR parameters, respectively, as a function of temperature for $\text{Yb}_{1-x}\text{Gd}_x\text{Fe}_2\text{Zn}_{20}$ ($0 \lesssim x \leq 0.05$).

and

$$b = \frac{d(\Delta H)}{dT} = \frac{\pi k_B}{g\mu_B} [\langle J_{f,ce}^2(q) \rangle_F \eta_F^2], \quad (2)$$

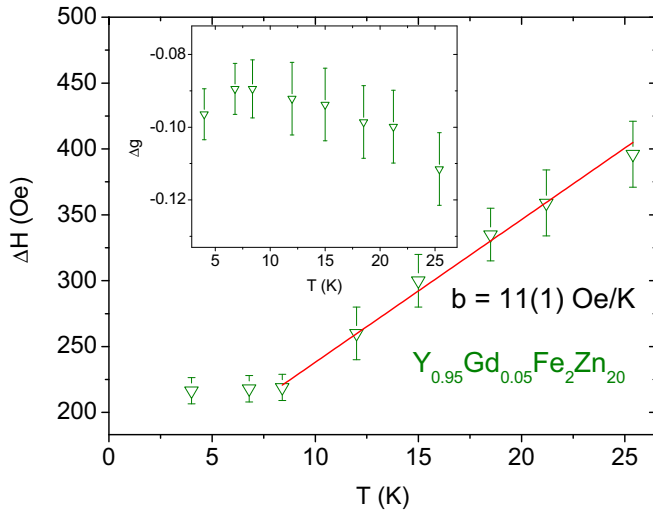


FIG. 6. Extracted ΔH and Δg (inset) as a function of temperature for $Y_{0.95}Gd_{0.05}Fe_2Zn_{20}$.

where $J_{f,ce}(0)$ is the effective exchange parameter between Gd^{3+} and ce in the absence of ce momentum transfer, η_F is the “bare” density of states at the Fermi surface, $\langle J_{f,ce}^2(q) \rangle_F$ is the average over the Fermi surface of the square of the q -dependent effective exchange parameter in the presence of ce momentum transfer, $q = |k_{out} - k_{in}|$ [26], k_B is the Boltzmann constant, and μ_B is the Bohr magneton.

The linear T dependence of ΔH observed for our three samples ($\Delta H = a + bT$) implies a Korringa relaxation rate, b , almost unaltered with the Gd^{3+} concentration [Fig. 5(c)]. This allows us to use the Hasegawa dynamic model in the *unbottleneck* regime for analysis of the exchange-coupled localized magnetic moment and ce [27].

Previously reported data on intermediate valence systems, as was the case of $YbInCu_4$, reveals a contribution of the RKKY interaction between Gd^{3+} and Yb^{3+} in the linewidth at relatively high temperatures and high concentrations [28]. This extra contribution due to the ce polarization mechanisms may be manifested in our system, especially for the $x = 0.05$ sample, and will be explored in further investigations.

The T dependence of both Δg and ΔH for $x = 0.05$ [Figs. 5(b) and 5(c)] separates the sample response in two regimes: a high- T ($T > 25$ K) noninteracting paramagnetic regime and a low- T ($T < 25$ K) regime with interacting magnetic ions. Note that below the Kondo temperature $T_K \approx 32$ K, the Yb ions become screened by ce , losing their localized magnetic moments and allowing us to ignore direct Gd-Yb interactions. In the high- T paramagnetic region ($T \gtrsim T_K$), the ESR data for this sample gives $b \sim 50(3)$ Oe/K and, concomitantly, shows $\Delta g \sim -0.10(4)$ as a representative value. For a single ce band at the Fermi level and absence of q dependence of the exchange interaction (i.e., absence of ce momentum transfer) [26], these two observables should be related as $b = \frac{\pi k_B}{g\mu_B} (\Delta g)^2$ [see Eqs. (1) and (2)]. From $\Delta g \sim -0.10$, we estimate $b \sim 234$ Oe/K, which is too large compared to the experimental value. This suggests a q dependence for the Gd- ce exchange parameter $J_{f,ce}(q)$.

Following the procedure described in previous work [16], using the above-discussed effective Sommerfeld coefficient $\gamma_{Yb:Gd}^{eff} = 480(6)$ mJ mol⁻¹ K² and within a free electron model approximation, we estimate $\eta_F = 101$ states eV⁻¹ fu spin. Then, a rough estimate of the exchange parameter gives $J_{f,ce}(0) = -0.99(6)$ meV and $\langle J_{f,ce}(q) \rangle_F = 0.46(6)$ meV in the paramagnetic regime (away from correlation effects). These values are smaller than the ones obtained for $GdFe_2Zn_{20}$ [$J_{Gd-ce}(0) = -20$ meV and $\langle J_{Gd-ce}(q) \rangle_F = 11.4$ meV] [16], which is expected given the stronger long-range magnetic interaction and higher ordering temperature in the latter system.

It is worth mentioning that for our reference compound of $Y_{0.95}Gd_{0.05}Fe_2Zn_{20}$, we found $b \sim 11$ Oe/K (Fig. 6). Therefore the enhancement of the relaxation process due to the Yb itinerant $4f$ - ce is about fivefold, revealing the enhanced density of states at the Fermi level. We should also mention that for samples with Gd content $x = 0.005$ and 0.01 in YFe_2Zn_{20} a resonance with a strong ce character was observed. These observations will be a subject of a future detailed report and we argue here that they do not affect the analysis of the Gd^{3+} ESR in the $YbFe_2Zn_{20}$ system.

We now focus on the low- T region ($T \lesssim T_K$), where ΔH and Δg present quite different T and Gd concentration dependence (Fig. 5), reflecting a correlated regime that we shall attempt to elucidate. Under this regime, ΔH shows a thermal broadening similar to that in the paramagnetic region for the highly diluted Gd samples [Fig. 5(c)] but for $x = 0.05$, the low- T ΔH tends to level off towards a constant, concentration-dependent, residual inhomogeneous linewidth, ΔH_{res} . Thus the thermal broadening of ΔH points out the presence of a Korringa relaxation for the low- T and the absence of strong magnetic interaction effects.

Furthermore, for the low-concentration samples, Δg is negative, small, and T -dependent [Fig. 5(b)], whereas for the $x = 0.05$ sample, Δg is not only strongly T -dependent, but changes sign. Hence, below T_K , the Hasegawa dynamic model cannot be applied to this system in a straightforward manner. Here, a negative T -dependent Δg for the lowest concentration samples suggests the presence of an internal T -dependent

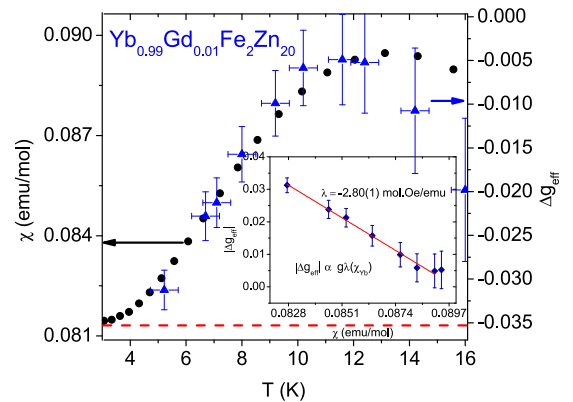


FIG. 7. Comparison of the temperature dependence of the dc magnetic susceptibility and effective g shift for $Yb_{0.99}Gd_{0.01}Fe_2Zn_{20}$. The inset shows how the latter relates to the susceptibility following the molecular field model (see text).

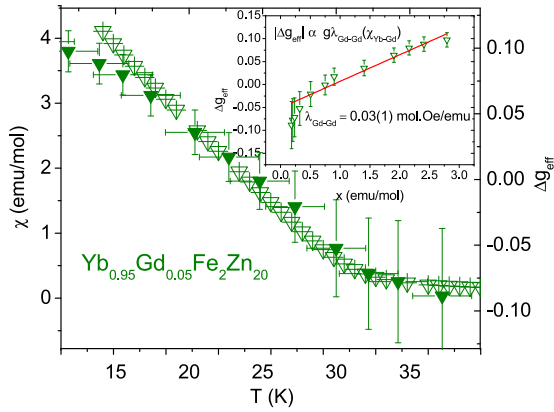


FIG. 8. Direct-current magnetic susceptibility and Δg as a function of temperature for $\text{Yb}_{0.95}\text{Gd}_{0.05}\text{Fe}_2\text{Zn}_{20}$. The inset shows Δg_{eff} vs $\chi_{\text{Yb:Gd}}$ following $g_{\text{eff}} = g[1 + \lambda^* \chi_{\text{Yb:Gd}}]$.

AFM field, whereas the sign change for the $x = 0.05$ sample reflects the onset of an internal T -dependent FM magnetic field below T_K , in accordance with the magnetization data.

To complete our analyses of the T -dependent Δg trends shown in Fig. 5(b), we select $\text{Yb}_{0.99}\text{Gd}_{0.01}\text{Fe}_2\text{Zn}_{20}$ to represent the low concentration samples. Since the magnitude of the negative Δg increases for $T \lesssim 12$ K, it is evident that a T -dependent AFM *internal field* is shifting the Gd^{3+} resonance toward higher applied external fields (also observed for the $x = 0.005$ sample). We describe this internal field in terms of a molecular field model, driven by the magnetic susceptibility of the Kondo system $\text{YbFe}_2\text{Zn}_{20}$ (χ_{Yb}), which leads to $g_{\text{eff}} = g(1 + \lambda \chi_{\text{Yb}})$ [29], where λ is the molecular field constant. This scaling, $\Delta g_{\text{eff}} \propto g \lambda \chi_{\text{Yb}}$, is strongly supported by the very similar T dependence of both Δg and χ_{Yb} (see Fig. 7) showing the same maximum at $T \lesssim 12$ K. Then, plotting $|\Delta g_{\text{eff}}|$ as a function of χ_{Yb} (inset of Fig. 7), we extract the molecular field parameter $\lambda = -2.8(1)$ mol Oe emu^{-1} in $\text{Yb}_{0.99}\text{Gd}_{0.01}\text{Fe}_2\text{Zn}_{20}$, which we attribute to the screening of the Yb^{3+} local moments by *ce* polarization as the Kondo condensate sets in at low T .

This comparison also allows to estimate $\Delta g_{\text{eff}} = -0.038(5)$ associated to a χ_{Yb} (red dotted line in the lower part of the main graph) as the system adopts an enhanced Fermi-liquid ground state below $T \approx 2$ K, from the $4f$ -*ce* hybridization. This estimated low- T g shift leads to a Korringa relaxation of $b = 35(8)$ Oe/K, which is, surprisingly, comparable to the measured values for our three samples, indicating little or no q dependence in the exchange interaction. Hence these results suggest that the Fermi surface should undergo a reconstruction process from $T > T_K$ (strong q dependence of the exchange) to $T < T_K$ (absence of q dependence).

Finally, for the higher concentration sample, $\text{Yb}_{0.95}\text{Gd}_{0.05}\text{Fe}_2\text{Zn}_{20}$, the T -dependent Δg displayed in Fig. 5(b) shows a strong positive increase at low T . In

contrast with the low concentration samples, here, it is evident that a T -dependent FM internal field is shifting the Gd^{3+} resonance toward lower applied fields. We shall again describe this internal field in terms of a molecular field driven by the magnetic susceptibility [Fig. 2(a)] of this sample, and proceed to a similar analysis of $g_{\text{eff}} = g(1 + \lambda^* \chi_{\text{Yb:Gd}})$ as shown in Fig. 8. This analysis gives a molecular field parameter $\lambda^* = 0.03(1)$ mol Oe emu^{-1} that accounts for the Gd-Gd interaction. The difference between λ (Yb-Kondo condensate) and λ^* (Gd-FM state) naturally reflects the nature of the interactions involved in their magnetic susceptibilities. We thus conclude that the progressive Gd substitution in this system has allowed the tuning of an interplay between short-range Kondo-like and long-range FM superexchange-like magnetic interactions.

V. CONCLUSIONS

In this work, we have shown that very low substitution levels of hybridizing Yb^{3+} ions by magnetically localized Gd^{3+} ions, in the Kondo-lattice compound $\text{YbFe}_2\text{Zn}_{20}$, allow tuning of a subtle low- T coexistence and competition between a Kondo condensate and a ferromagnetic ground state.

Our experimental data reveal two very distinct regimes, with crossover driven by the Kondo temperature ($T_K \approx 32$ K) and the Gd concentration. For higher Gd concentration ($x \approx 0.05$) and $T \gtrsim T_K$, the system behaves as a regular metallic paramagnet where the Fermi surface allows for a q dependence of the exchange interaction between the localized Gd^{3+} ions and the *ce*. Conversely, for low Gd concentrations ($x \lesssim 0.01$) and $T \lesssim T_K$, a noticeable coexistence of two competing magnetic states is evident, a Kondo AFM-like state and a FM one. Under this regime, our Gd^{3+} ESR experiments suggest that the Fermi surface undergoes a reconstruction process where the exchange interaction between the Gd^{3+} ions and the *ce* does not depend on the *ce* momentum transfer, i.e., there is no significant q dependence of the exchange interaction ($J_{f-ce}(0) = \langle J_{f-ce}(q) \rangle_F$). We were also able to apply a molecular field model to calculate the molecular field parameter in the Kondo condensate state (low x) and for FM interactions (high x).

In summary, our low- T Gd^{3+} ESR experiments were able to probe important features characteristic of a Kondo system doped with magnetic impurities, which tends to experience FM coupling. We point out that it has been proven possible to extract microscopic information using ESR experiments in a strongly correlated system, by tuning the competition between long- and short-range magnetic interactions.

ACKNOWLEDGMENTS

This work was supported by Brazilian agencies FAPESP (Grants No. 2016/15780-0 and No. 2011/19924-2), CNPq, CAPES, and FINEP. The authors are grateful to the Multiuser Central Facilities (UFABC) for the experimental support.

[1] G. R. Stewart, *Rev. Mod. Phys.* **56**, 755 (1984).
[2] G. R. Stewart, *Rev. Mod. Phys.* **73**, 797 (2001).

[3] G. R. Stewart, *Rev. Mod. Phys.* **78**, 743 (2006).
[4] J. Kondo, *Prog. Theor. Phys.* **32**, 37 (1964).

- [5] M. S. Torikachvili, S. Jia, E. D. Mun, S. T. Hannahs, R. C. Black, W. K. Neils, Dinesh Martien, S. L. Bud'ko, and P. C. Canfield, *Proc. Natl. Acad. Sci. USA* **104**, 9960 (2007).
- [6] E. T. Magnavita, C. Rettori, J. M. Osorio-Guillén, F. F. Ferreira, L. Mendonça-Ferreira, M. A. Avila, and R. A. Ribeiro, *J. Alloys Compd.* **669**, 60 (2016).
- [7] K. Shigetoh, D. Hirata, M. A. Avila, and T. Takabatake, *J. Alloys Compd.* **403**, 15 (2005).
- [8] M. A. Avila, M. Sera, and T. Takabatake, *Phys. Rev. B* **70**, 100409 (2004).
- [9] W. B. Jiang, L. Yang, C. Y. Guo, Z. Hu, J. M. Lee, M. Smidman, Y. F. Wang, T. Shang, Z. W. Cheng, F. Gao, H. Ishii, K. D. Tsuei, Y. F. Liao, X. Lu, L. H. Tjeng, J. M. Chen, and H. Q. Yuan, *Sci. Rep.* **5**, 17608 (2015).
- [10] T. Tanaka and Y. Kubo, *J. Phys. Soc. Jpn.* **79**, 124710 (2010).
- [11] M. Cabrera-Baez, R. A. Ribeiro, and M. A. Avila, *J. Phys.: Condens. Matter* **28**, 375601 (2016).
- [12] A. Abragam and B. Bleaney, *Electron Paramagnetic Resonance (EPR) of Transition Ions* (Clarendon, Oxford, UK, 1970).
- [13] S. E. Barnes, *Adv. Phys.* **30**, 801-938 (1981).
- [14] R. H. Taylor, *Adv. Phys.* **24**, 681 (1975).
- [15] M. Cabrera-Baez, A. Naranjo-Urbe, J. M. Osorio-Guillén, C. Rettori, and M. A. Avila, *Phys. Rev. B* **92**, 214414 (2015).
- [16] M. Cabrera-Baez, A. Naranjo-Urbe, J. M. Osorio-Guillén, C. Rettori, and M. A. Avila, *Phys. Rev. B* **95**, 104407 (2017).
- [17] J. Korryng, *Physica* **16**, 601 (1950).
- [18] R. A. Ribeiro and M. A. Avila, *Philos. Mag.* **92**, 2492 (2012).
- [19] P. C. Canfield and Z. Fisk, *Philos. Mag.* **65**, 1117 (1992).
- [20] T. Nasch and W. Jeitschko, and U. C. Rodewald, *Z. Naturforsch. B* **52**, 1023 (1997).
- [21] S. Jia, N. Ni, S. L. Bud'ko, and P. C. Canfield, *Phys. Rev. B* **76**, 184410 (2007).
- [22] G. Feher and A. F. Kip, *Phys. Rev.* **98**, 337 (1955).
- [23] F. J. Dyson, *Phys. Rev.* **98**, 349 (1955).
- [24] S. Jia, N. Ni, G. D. Samolyuk, A. Safa-Sefat, K. Dennis, H. Ko, G. J. Miller, S. L. Bud'ko, and P. C. Canfield, *Phys. Rev. B* **77**, 104408 (2008).
- [25] M. Cabrera-Baez, W. Iwamoto, E. T. Magnavita, J. M. Osorio-Guillén, R. A. Ribeiro, M. A. Avila, and C. Rettori, *J. Phys.: Condens. Matter* **26**, 175501 (2014).
- [26] D. Davidov, K. Maki, R. Orbach, C. Rettori, and E. P. Chock, *Solid State Commun.* **12**, 621 (1973).
- [27] H. Hasegawa, *Prog. Theor. Phys.* **21**, 483 (1959).
- [28] T. S. Altshuler, M. S. Bresler, M. Schlott, B. Elschner, and E. Gratz, *Z. Phys. B: Condens. Matter* **99**, 57 (1995).
- [29] J. G. S. Duque, E. M. Bittar, C. Adriano, C. Giles, L. M. Holanda, R. Lora-Serrano, P. G. Pagliuso, C. Rettori, C. A. Pérez, Rongwei Hu, C. Petrovic, S. Maquilon, Z. Fisk, D. L. Huber, and S. B. Oseroff, *Phys. Rev. B* **79**, 035122 (2009).